Clinical
Cancer
Research

B-Cell Lymphoma Patient-Derived Xenograft Models Enable Drug Discovery and Are a Platform for Personalized Therapy

Leo Zhang[1], Krystle Nomie[1], Hui Zhang[1], Taylor Bell[1], Lan Pham[2], Sabah Kadri[3], Jeremy Segal[3], Shaoying Li[2], Shouhao Zhou[4], David Santos[5], Shawana Richard[1], Shruti Sharma[3], Wendy Chen[1], Onyekachukwu Oriabure[1], Yang Liu[1], Shengjian Huang[1], Hui Guo[1], Zhihong Chen[1], Wenjing Tao[1], Carrie Li[1], Jack Wang[1], Bingliang Fang[6], Jacqueline Wang[6], Lei Li[7,8], Maria Badillo[1], Makhdum Ahmed[1], Selvi Thirumurthi[9], Steven Y. Huang[10], Yiping Shao[11], Laura Lam[1], Qing Yi[12], Y. Lynn Wang[3], and Michael Wang[1,13]

Abstract

Purpose: Patients with B-cell lymphomas often relapse after frontline therapy, and novel therapies are urgently needed to provide long-term remission. We established B-cell lymphoma patient-derived xenograft (PDX) models to assess their ability to mimic tumor biology and to identify B-cell lymphoma patient treatment options.

Experimental Design: We established the PDX models from 16 patients with diffuse large B-cell lymphoma, mantle cell lymphoma, follicular lymphoma, marginal zone lymphoma, or Burkitt lymphoma by inoculating the patient tumor cells into a human bone chip implanted into mice. We subjected the PDX models to histopathologic and phenotypical examination, sequencing, and drug efficacy analysis. Primary and acquired resistance to ibrutinib, an oral covalent inhibitor of Bruton tyrosine kinase, were investigated to elucidate the mechanisms underlying ibrutinib resistance and to identify drug treatments to overcome resistance.

Results: The PDXs maintained the same biological, histopathologic, and immunophenotypical features, retained similar genetic mutations, and produced comparable drug responses with the original patient tumors. In the acquired ibrutinib-resistant PDXs, PLC-γ2, p65, and Src were downregulated; however, a PI3K signaling pathway member was upregulated. Inactivation of the PI3K pathway with the inhibitor idelalisib in combination with ibrutinib significantly inhibited the growth of the ibrutinib-resistant tumors. Furthermore, we used a PDX model derived from a clinically ibrutinib-relapsed patient to evaluate various therapeutic choices, ultimately eliminating the tumor cells in the patient's peripheral blood.

Conclusions: Our results demonstrate that the B-cell lymphoma PDX model is an effective system to predict and personalize therapies and address therapeutic resistance in B-cell lymphoma patients. *Clin Cancer Res; 23(15); 4212–23. ©2017 AACR.*

Introduction

Lymphoma is the most common hematologic malignancy, and B-cell lymphoma accounts for 85% of all lymphomas (1). The majority of B-cell lymphoma patients respond to initial therapy; however, most eventually relapse due to the development of therapeutic resistance (2, 3). Thus, an improved understanding

of the biology of relapsed/refractory B-cell lymphoma is critically needed to develop alternative treatment strategies for these patients (4–6).

The evaluation of novel drug targets using established B-cell lymphoma cell lines is limited by the inexact correlation between responsiveness observed in the cell line versus the patient sample (7). Similarly, "xenograft" models wherein human cancer cell

[1]Department of Lymphoma and Myeloma, The University of Texas MD Anderson Cancer Center, Houston, Texas. [2]Department of Hematopathology, The University of Texas MD Anderson Cancer Center, Houston, Texas. [3]Divison of Genomic and Molecular Pathology, Department of Pathology, The University of Chicago, Chicago, Illinois. [4]Department of Biostatistics, The University of Texas MD Anderson Cancer Center, Houston, Texas. [5]Department of Surgical Oncology, The University of Texas MD Anderson Cancer Center, Houston, Texas. [6]Department of Thoracic Surgery, The University of Texas MD Anderson Cancer Center, Houston, Texas. [7]Department of Experimental Radiation Oncology, Division of Radiation Oncology, The University of Texas MD Anderson Cancer Center, Houston, Texas. [8]Department of Genetics, The University of Texas MD Anderson Cancer Center, Houston, Texas. [9]Department of Gastroenterology, The University of Texas MD Anderson Cancer Center, Houston, Texas. [10]Department of Interventional Radiology, The University of Texas MD Anderson Cancer Center, Houston, Texas. [11]Department of Imaging Physics, The University of Texas MD

Anderson Cancer Center, Houston, Texas. [12]Department of Cancer Biology, Lerner Research Institute, Cleveland Clinic, Cleveland, Ohio. [13]Department of Stem Cell Transplantation and Cellular Therapy, The University of Texas MD Anderson Cancer Center, Houston, Texas.

Note: Supplementary data for this article are available at Clinical Cancer Research Online (http://clincancerres.aacrjournals.org/).

L. Zhang, K. Nomie, and M. Wang contributed equally to this article.

Corresponding Author: Michael Wang, The University of Texas MD Anderson Cancer Center, 1515 Holcombe Boulevard, Houston, TX 77030. Phone: 713-792-2860; Fax: 713-563-5067; E-mail: miwang@mdanderson.org

AACR

Translational Relevance

The B-cell lymphoma patient-derived xenograft (PDX) model recapitulated several biological, histopathologic, and clinical features of the original patient tumor. DNA sequencing of two B-cell lymphoma PDX mouse models demonstrated that these models most likely maintained the original mutations of the patient tumors. Interestingly, the PDX model mimicked the transient lymphocytosis observed among relapsed/refractory MCL patients treated with ibrutinib, further demonstrating the remarkable ability of this model to recapitulate patient biology. Furthermore, we established ibrutinib primary and acquired resistance PDX models and found novel combination therapies to overcome drug resistance in vivo. Of note, the PDX models successfully guided therapy of a clinically refractory lymphoma patient, reducing the patient's lymphocytosis. These results indicate that PDX mouse models are a valid experimental platform that can be utilized in a clinical trial to select personalized therapies for B-cell lymphoma patients.

lines are transplanted into immunocompromised mice do not represent the full spectrum of cancers because (i) the cell lines are not derived from patients, and (ii) the model lacks the tumor microenvironment in vivo. In contrast, patient-derived xenografts (PDX) possess both of these refinements. Unlike the cell line–derived tumor models, PDX mouse models contain heterogeneous tumor cell populations (8) similar to the patient tumor cell population, including possible cancer stem cells (9). Recent studies have indicated that PDX models can also recapitulate the treatment responses of the parental tumor and can be used to predict the choice of therapeutic target and regimen (10–13). Therefore, PDX models provide a valid experimental platform to assess the biology and progression of B-cell lymphoma and its response/resistance to novel therapeutic agents.

We previously established the first mantle cell lymphoma (MCL) PDX model with cells isolated from a patient then transplanted into a human fetal bone chip implanted in the mice to investigate MCL biology and drug responses (14). In this PDX model, the primary MCL tumor metastasized to the lymph nodes, spleen, bone marrow, and gastrointestinal tract of the host mice, mimicking MCL clinical features. Bone marrow involvement has been reported in diffuse large B-cell lymphoma (DLBCL; ref. 15), follicular lymphoma (FL; ref. 16), marginal zone lymphoma (MZL; ref. 17), and Burkitt lymphoma (BL; ref. 18), with a significantly poor prognosis for patients with this involvement (19, 20). Thus, we developed various B-cell lymphoma PDX models and recapitulated the pathological and clinical characteristics, molecular profiles, disease progression, and response to therapeutic agents in these B-cell lymphoma PDXs. Our results indicate that PDX mouse models are an indispensable tool towards personalized treatment for B-cell lymphoma.

Materials and Methods

Patient samples, drugs, and agents

Peripheral blood, apheresis, biopsy tissues isolated from spleen and lymph nodes, bone marrow aspirates, ascites, or pleural effusion were obtained from B-cell lymphoma patients who provided informed consent. The sample collection protocol was approved by the Institutional Review Board at The University of Texas MD Anderson Cancer Center. All procedures were conducted in accordance with the Declaration of Helsinki. Mononuclear cells were separated by Ficoll-Hypaque density centrifugation, and tumor cells were isolated using anti-CD19 antibody-coated magnetic microbeads (Miltenyi Biotec) and maintained in RPMI1640 medium (Life Technologies) supplemented with 10% heat-inactivated FBS, penicillin (10,000 U/mL, Sigma), streptomycin (10 mg/mL, Sigma), and L-glutamine (29.2 mg/mL, Life Technologies). These isolated tumor cells were used for molecular profiling, in vitro experiments, and inoculation into mice. The drugs or agents used for the in vitro or in vivo drug assays are listed in Supplementary Table S1.

B-cell lymphoma-bearing PDX mouse models

Six- to 8-week-old male CB-17 SCID mice (Harlan) or NSG (Nod SCID Gamma) mice (The Jackson Laboratory) were housed and monitored in our animal research facility. All experimental procedures and protocols were approved by the Institutional Animal Care and Use Committee of The University of Texas MD Anderson Cancer Center. Fresh human fetal bones of 17 to 19 gestational weeks (Advanced Bioscience Resources) were subcutaneously implanted into SCID or NSG mice (SCID/NSG-hu). Approximately 4 to 6 weeks following implantation, 5×10^6 freshly isolated lymphoma cells were directly injected into human fetal bone implants within SCID/NSG-hu hosts after the mice were anesthetized with 5% isoflurane vaporizer. Mouse serum was collected, and the levels of circulating human β_2M in mouse serum [human β_2-microglobulin (β_2M) ELISA Kit (Abnova Corporation)] were used to monitor tumor engraftment and burden. Once tumor growth was detected in the first generation (G), the mice were sacrificed, and tumor masses were isolated. The tumor cells were tested for human CD20 expression and then inoculated in NSG mice as the second generation (G2). Isolated G2 tumor cells were utilized for high-throughput drug screening. Meanwhile, the remaining tumor mass was cut into 3 mm³ sections that were then passaged into 10 to 20 NSG mice for next-generation (G3) tumor growth. From G3, the tumor mass was equally cut into 3 mm³ pieces and passaged into 20 to 50 NSG mice (3–5 mice/group, dependent on the experimental drug treatment) for in vivo treatment. During and after treatment with vehicle control or the indicated drugs, mouse serum was collected, and tumor burden was evaluated by measuring either human β_2M levels or tumor volume to determine therapeutic efficacy in the PDX models. Freshly isolated cells from the tumor mass of each generation and treatment group were labeled with FITC/PE-conjugated antihuman CD5, CD10, CD20, or CD45 mAb (BD Biosciences) to validate the population of human lymphoma cells by flow cytometry.

Histopathologic analysis

Excised tissues from patients and PDX mice were fixed in 10% formalin solution, processed by standard methods, embedded in paraffin, sectioned at 5 μm, and stained with H&E. For IHC evaluation, the tissues were stained with antibodies against human CD20, KI-67, Cyclin D1 or PAX5 (Dako), counterstained with Harris hematoxylin and examined by standard light microscopy. Samples were analyzed using an Olympus BX51TF microscope equipped with UPlan FL 40×/0.75 and 20×/0.50 objective lenses (Olympus).

In vitro drug screening

Tumor cells isolated from original patient samples and/or from different generations of PDX mice were utilized for high-throughput in vitro screening of potential drugs and their combinations using the CellTiter-Glo luminescent cell viability assay (Promega). Cells were seeded in triplicate in a 96-well plate with 2×10^5 cells per well and were treated with different combinations of potential therapeutic agents (Supplementary Table S1) for 48 hours. In the last 30 minutes, 50 µL of CellTiter 96 Aqueous One Solution Reagent were added to the culture wells and incubated at 37°C in 5% CO_2. Light absorbance of formazan was measured at 495 nm on a universal microplate reader equipped with KC4 software (Biotek Instruments).

^{18}F-fluorodeoxyglucose PET/CT imaging

After fasting for 8 to 12 hours, the PDX mice were imaged by microPET/CT under general anesthesia with 5% isoflurane vaporizer. The ^{18}F-fluorodeoxyglucose (^{18}F-FDG) biodistribution was evaluated with the Albira trimodal PET/SPECT/CT system [PET, SPECT (single photon emission CT), and CT).

Reverse-phase protein array assay

PDX tumors (3 mm^3) were incubated with 1% SDS (with beta-mercaptoethanol) and diluted in five 2-fold serial dilutions in lysis buffer containing 1% SDS. Serial diluted lysates were arrayed on nitrocellulose-coated slides (Grace Bio-lab) with the Aushon 2470 Arrayer (Aushon BioSystems). A total of 5,808 array spots were arranged on each slide, including the spots corresponding to positive and negative controls prepared from mixed cell lysates or dilution buffer, respectively. Each slide was probed with a validated primary antibody plus a biotin-conjugated secondary antibody. Only antibodies with a Pearson correlation coefficient between reverse-phase protein array assay (RPPA) and Western blotting of greater than 0.7 were used. Antibodies with a single or dominant band on Western blotting were assessed by direct comparison to RPPA using cell lines with differential protein expression or modulated with ligands/inhibitors or siRNA for phospho- or structural proteins, respectively. The antibodies used to probe the slides are listed in Supplementary Table S2. The signal obtained was amplified using a Dako Cytomation–catalyzed system (Dako) and visualized by DAB colorimetric reaction. The slides were scanned, analyzed, and quantified using customized Microvigene software (VigeneTech Inc.) to generate spot intensity. Each dilution curve was fitted with a logistic model ("Supercurve Fitting" developed by the Department of Bioinformatics and Computational Biology in MD Anderson Cancer Center). The fitted curve was plotted with the signal intensities, both observed and fitted, on the y-axis and the log2-concentration of proteins on the x-axis for diagnostic purposes. The protein concentrations of each slide set were normalized by median polish, which was corrected across samples by the linear expression values using the median expression levels of all antibody experiments to calculate a loading correction factor for each sample.

DNA sequencing using OncoPlus

OncoPlus is a 1,212 hybrid capture gene panel developed at the University of Chicago. The panel contains genes associated with cancer in both the somatic and inherited contexts, and utilizes a custom SeqCap EZ capture (Roche Applied Science) with 2×100 bp sequencing performed on an Illumina Hiseq-2500. Data were processed in customized computational pipelines using a combination of publicly available and customized software. The serial generations of PDX samples with the original patient samples were sequenced using OncoPlus. Approximately 1,500 variants were detected within the exonic territories of the 1,212 genes in each sample. These variants were then filtered on the basis of their 1000G frequencies (21) to remove common germ line SNPs, and their coding effects.

Statistical analysis

Multiple linear regression was applied to investigate drug treatment effects on the primary patient tumors and PDXs in vitro. Linear mixed-effects regression model was used to assess the change of human β_2M or $CD5^+CD20^+$ cells by treatment. Survival analysis was conducted by log-rank test. P values of <0.05 were considered statistically significant.

Results

Patient characteristics and the establishment of 16 B-cell lymphoma PDX models

We collected clinical samples from 16 patients with several types of B-cell lymphomas (Table 1), including MCL ($n = 8$), DLBCL ($n = 3$), FL ($n = 2$), BL ($n = 1$), and MZL ($n = 2$). In total, 25% of the patients had indolent lymphomas (4/16). Furthermore, of the 16 patients, 9 (56%) were newly diagnosed and untreated clinically, and 7 (44%) patients were relapsed after prior treatment with 1–3 chemotherapy or targeted therapy treatments. Of the 8 MCL patients, 4 (25%) patients were exposed to ibrutinib treatment after prior chemotherapies. In addition, 10 patients displayed bone marrow involvement as detected by bone marrow aspiration, except for PT6, PT9, and PT13 who displayed no evidence of bone marrow infiltration. No bone marrow aspirations were performed on PT4, PT12, and PT16. The clinical pathology reports showed TP53 deletion in PT5, Bcl-2 deficiency in PT2, and Bcl-2 and Bcl-6 rearrangement in PT16. These genetic changes may reflect refractoriness or may be potential molecular targets in both patients and PDXs.

Fresh lymphoma cells isolated from patient samples were injected into SCID/NSG-hu mice. A schema of the establishment and the application of the primary B-cell lymphoma PDX model are shown in Supplementary Fig. S1A. Human β_2M levels, an indicator of lymphoma tumor growth, increased progressively in the peripheral blood of PDX mice, reflecting the successful engraftment and subsequent growth of the patient tumors. The levels of circulating human β_2M after 3 weeks of patient tumor cell engraftment in the 16 B-cell lymphoma PDX mouse models showed successful tumor engraftment compared with the human β_2M levels in NSG or NSG-hu mice (Supplementary Fig. S1B, $P < 0.05$). The tumors cells from PT5 were inoculated into SCID-hu mice and were not passaged to next generations. Of the remaining 15 PDXs, 10 of 15 PDXs were serially passaged for more than six generations, indicating a 67% passage success rate.

Comparisons between the original patient tumors and PDX tumors

We investigated whether the PDXs of each generation possessed similar clinical, pathological, and molecular features as the original patient tumor. The histologic examination of nine generations of subcutaneous tumor masses of PT1 MCL-PDXs and PT2

Table 1. Characteristics of the patients for primary lymphoma PDX model

No.	Diagnosis	Age	Gender	Sample origin	Passage	Ibrutinib exposure	BM infiltration	Disease status	Prior therapy	Ki-67 (%)	LDH (IU/L)	β_2M (mg/L)
PT1	Mantle cell lymphoma	60	M	PB	11	No	Yes	Untreated	None	5–7	462	5.5
PT2	Burkitt lymphoma	37	M	Ascites	14	No	Yes	Untreated	None	100	656	7.6
PT3	Follicular lymphoma	42	F	Pleural effusion	2	No	Yes	Untreated	None	5	421	4.5
PT4	Marginal zone lymphoma	47	M	Spleen	2	No	NA	Untreated	None	NA	NA	NA
PT5	Mantle cell lymphoma	61	M	PB	No passage	No	Yes	Untreated	None	30	462	4.9
PT6	Diffuse large B-cell lymphoma	65	M	Pleural effusion	2	No	No	Treated	R-EPOCH[a]	50–60	561	1.8
PT7	Marginal zone lymphoma	63	M	PB	8	No	Yes	Treated	R[a]	NA	348	2.2
PT8	Mantle cell lymphoma	84	M	Pheresis	9	Yes	Yes	Treated	R-CHOP, velcade, ibrutinib	60–70	2868	NA
PT9	Follicular lymphoma	34	F	Excision biopsy	7	No	No	Untreated	None	<5%	456	1.7
PT10	Mantle cell lymphoma	74	F	Excision biopsy	10	Yes	Yes	Treated	R-Bendamustine-methotrexate, R-hyperCVAD, ibrutinib-rituximab	30	739	5.4
PT11	Mantle cell lymphoma	48	F	PB	10	No	Yes	Untreated	None	5–10%	638	3.0
PT12	Diffuse large B-cell lymphoma	51	M	Excision biopsy	10	No	NA	Untreated	None	60–70	996	3.5
PT13	Mantle cell lymphoma	76	M	Core biopsy	2	Yes	No	Treated	R-Bendamustine, R-ibrutinib, Radiotherapy	5–10	868	3.7
PT14	Mantle cell lymphoma	60	M	Pheresis	2	No	Yes	Untreated	None	NA	233	4.9
PT15	Mantle cell lymphoma	88	F	PB	6	Yes	Yes	Treated	R-CHOP, R-Bendamustine, R-Bortezomib, ibrutinib	30–50	998	3.4
PT16	Diffuse large B-cell lymphoma	39	M	Ascites	8	No	NA	Treated	R-CHOP, RICE	NA	2530	NA

Abbreviations: β_2M, beta-2-microglobulin; BM, bone marrow; LDH, lactate dehydrogenase; NA, not available; PB, peripheral blood; R, rituximab; R-CHOP, rituximab plus cyclophosphamide, vincristine, doxorubicin, and prednisone; R-EPOCH, rituximab plus etoposide, cyclophosphamide, vincristine, doxorubicin, and prednisone; RICE, rituximab plus ifosfamide, carboplatin, and etoposide.
[a]The patient received only one dose of treatment before sample collection.

BL-PDXs indicated consistent tumor features in each generation (Supplementary Fig. S2A). Once the tumors grew in the subcutaneous implant sites, the tumors frequently metastasized to the mouse spleen, mimicking disease progression in humans (Supplementary Fig. S2B and S2C). Specifically, PET/CT scans of PT1 and PT5 diagnosed splenomegaly in the clinic (Supplementary Fig. S2D, left), which was also observed in the respective patient PDXs (PT1-G3 NSG mice and PT5-G1 SCID-hu mice; Supplementary Fig. S2D, middle). Furthermore, H&E staining showed the characteristic histology of human lymphoma cells in the spleens of PT1-G3 and PT5-G1 PDX mice (Supplementary Fig. S2D, right).

Next, to investigate the immunologic and pathologic characteristics between the patient tumors and their respective PDX tumors, immunophenotype and IHC data were extracted from our patient clinical database and were compared with the PDX immunophenotype and IHC PDX findings. The representative data of five models (PT2-BL-G12, PT7-MZL-G6, PT8-MCL-G2, PT10-MCL-G3, and PT12-DLBCL-G3) displayed the same immunophenotypes (Fig. 1A) and anti-human CD20-positive staining (Fig. 1B) as their original patient tumors. In addition, anti-human PAX5-positive staining of PT2-BL and PT10-MCL also matched the original patient tumor staining results (Fig. 1C). Meanwhile, the percentage of human cyclin D1- and Ki-67–expressing cells was consistent between the two MCL PDXs (PT8-MCL and PT10-MCL) and their respective patient samples (Fig. 1D).

Using the OncoPlus Universal Cancer Mutation Analysis Panel, we identified the same mutations in 1,212 cancer-associated genes between the patient primary tumors and PT8-MCL and PT10-MCL PDX-generated tumors across multiple generations. As a result, each sample had approximately 55 variants, which included somatic variants as well as some rare SNPs that cannot be distinguished as a matched normal was not sequenced. The somatic variants included pathogenic drivers as well as passenger
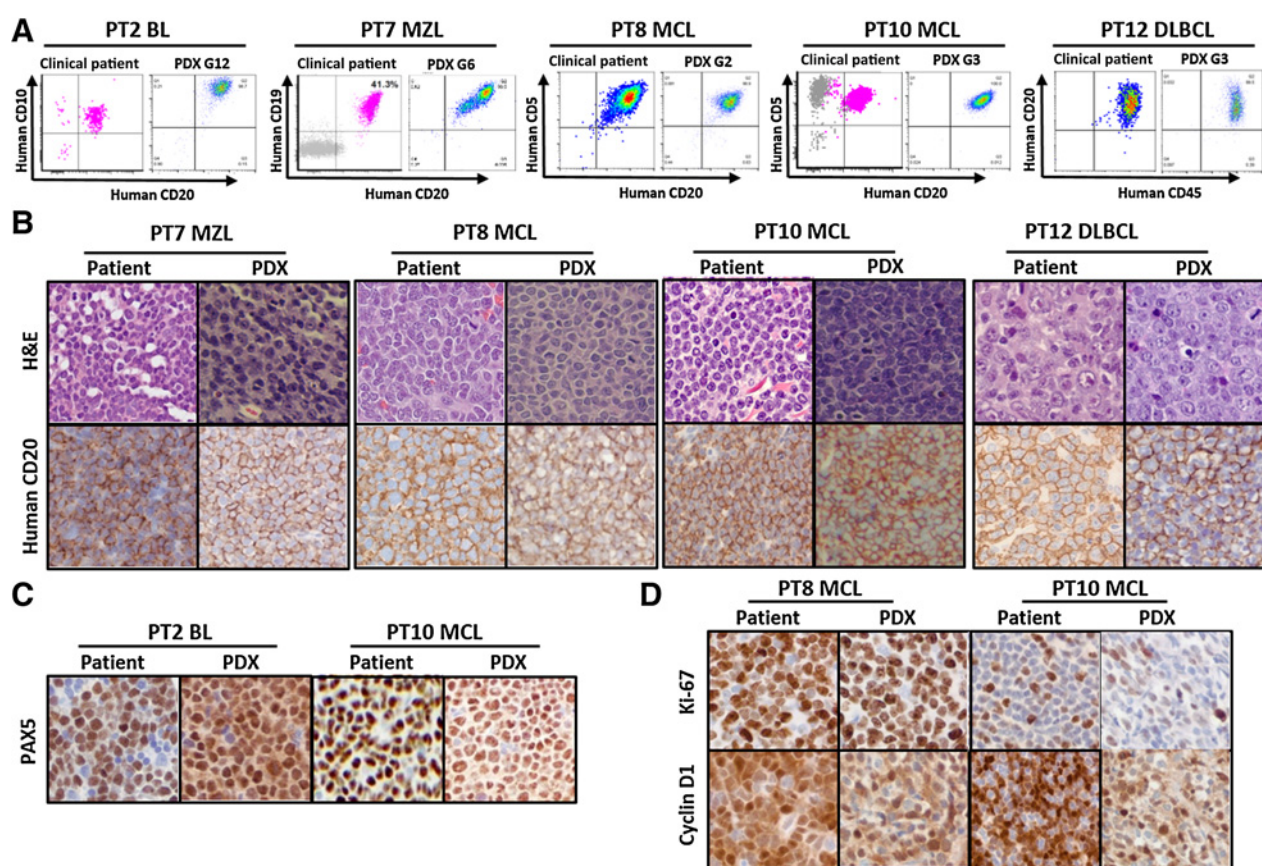
Figure 1.
Immunophenotyping and histopathological characterization of the PDX models in comparison with the original patient tumors. **A,** Immunophenotypes of PDX tumors compared with the primary tumors from patients with different B-cell lymphoma subtypes. **B,** H&E staining and anti-human CD20 IHC staining of the original patient tumors and their PDXs. Human PAX5 (**C**), and Human Ki-67 and cyclin D1 staining (**D**) of the original patient tumors and their PDXs. H&E and IHC image magnification, ×400. PT, patient.

mutations of uncertain significance. A list of all variants detected by UCM-OncoPlus in the primary tissue is shown in Supplementary Table S3. Only one additional mutation was identified in PT8-MCL-G3. Specifically, PT8-MCL-G3 gained a Thr1627Met mutation in *DNAH5* at 20% allele frequency. The *DNAH5* mutation has not been reported to be associated with B-cell lymphoma. On the basis of this analysis, these two representative PDX mouse models appear to maintain original patient mutations of these specific 1,212 cancer-associated genes without the loss or accumulation of additional mutations (Fig. 2).

Reproduction of the clinical compartmental shift phenomenon and the identification of novel combination therapy in PDX mice

In the phase II ibrutinib single-agent clinical trial, we observed ibrutinib-induced "compartmental shift" (lymphocytosis) of tumor cells from the primary tumor site into the peripheral blood in 34% of MCL patients treated with ibrutinib, an oral covalent inhibitor of Bruton tyrosine kinase (BTK; ref. 22). Here, we imitated this phenomenon in PT5-MCL-bearing PDX mice. The patient PT5 tumor cells were inoculated into the human fetal bone chip of SCID-hu mice. Three-week posttumor inoculation, these

mice were administered ibrutinib (25 mg/kg oral gavage daily). A transient increase of human $CD5^+CD20^+$ cells in the mouse peripheral blood was detected by flow cytometry on day 10 of treatment in the ibrutinib-treated group but not in the control group, representing an ibrutinib-induced shift of human MCL cells from the implanted bone chip (primary tumor site) to the mouse peripheral blood (Fig. 3A and B). Specifically, approximately 50% cells were human CD20-positive in the peripheral blood on day 10 of ibrutinib treatment, but these cells were not observed in the peripheral blood of control animals ($P < 0.0001$ between vehicle control and ibrutinib groups at day 10). These findings suggest that we were effectively able to recapitulate the biology of the human disease using the PDX mouse model.

In addition, once the ibrutinib-induced transient increase of human $CD5^+CD20^+$ cells in the mouse peripheral blood was detected, the MCL-bearing SCID-hu mice were treated with ibrutinib plus rituximab to determine whether this combination increased survival and reduced tumor burden compared with single agent therapy. This combination was utilized because we hypothesized that targeting CD20 with rituximab while simultaneously targeting BTK with ibrutinib would produce greater anticancer effects *in vivo*. The MCL-bearing G1 mice were divided
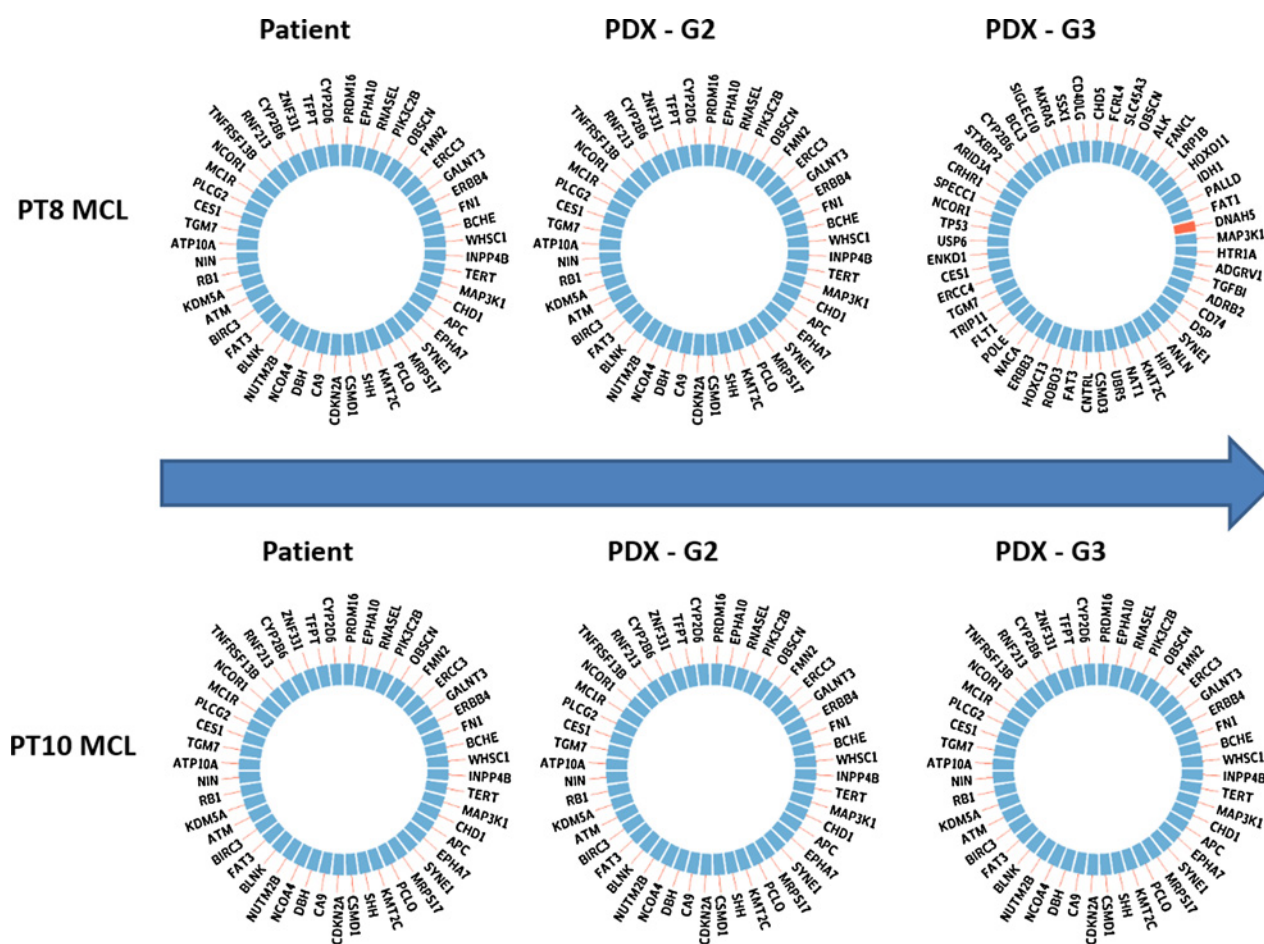
Figure 2.
Genetic comparisons between different PDX generations and the original patient tumors. Genetic fidelity was analyzed among the original patient tumor, PDX-G2, and PDX-G3 of PDXs in PT8 and PT10. A total of 1,212 cancer-associated genes were sequenced using OncoPlus. No mutational changes were found except for a *DNAH5* mutation found in PT8-PDX-G3, which gained a Thr1627Met mutation in *DNAH5* at 20% allele frequency.

into the following four groups: vehicle control, ibrutinib treatment alone, rituximab treatment alone, and ibrutinib and rituximab combination treatment. Rituximab was intravenously administered at 10 mg/kg every 3 days for a total of 7 doses. Tumor burden was monitored by assessing human β_2M levels in the mouse serum before combination treatment (day 0) and after treatment (day 30). The rituximab and ibrutinib combination reduced the human β_2M levels to almost undetectable levels compared with either single agent group or the vehicle control group (Fig. 3C, $P < 0.01$, ibrutinib plus rituximab vs. vehicle control or rituximab; $P < 0.05$, ibrutinib plus rituximab vs. ibrutinib). Furthermore, ibrutinib markedly increased the overall survival of the MCL-bearing mice compared with vehicle control ($n = 5$) or rituximab alone ($n = 5$). Importantly, all mice treated with ibrutinib plus rituximab ($n = 5$) survived at least 90 days after beginning combination therapy (Fig. 3D, $P = 0.0027$ for ibrutinib + rituximab vs. rituximab alone; $P = 0.0026$ for ibrutinib plus rituximab vs. vehicle control and $P = 0.134$ for ibrutinib + rituximab vs. IBN alone). These results demonstrate the marked effects of this combination in promoting survival in MCL-bearing PDX mice. On the basis of these preclinical data, ibrutinib plus

rituximab was investigated and found to be an effective regimen in a clinical trial with relapsed or refractory MCL patients (23).

B-cell lymphoma PDX models provide a platform to screen-targeted drug treatments

We next investigated whether the primary patient tumors and PDXs displayed similar responses to drug treatment *in vitro*. As shown in Fig. 4, freshly isolated PT2-BL cells from the original patient sample (Fig. 4A), from the G1 SCID-hu mouse (Fig. 4B), and from the G2 NSG mouse (Fig. 4C) were treated with a panel of drugs: ibrutinib, BGB-3111, carfilzomib, ABT-199, Cal-101 (idelalisib), and KPT-330 at different doses. All of the tumor cells, from both the patient and PDXs, showed the same drug response pattern. Of note, PT2-BL primary tumor cells were mostly resistant to the BCL-2 inhibitor ABT-199 (Fig. 4A), which may be explained by the *Bcl-2* deficiency identified in the PT2-BL clinical pathology report (data not shown). Importantly, the PDX tumors from both PT2-BL-G1 and PT2-BL-G2 were also resistant to ABT-199 (Fig. 4B and C); even after multiple passages to G6 and G7, the PT2-BL PDX model still maintained resistance to ABT-199 (Supplementary Fig. S3), indicating that the PDXs most likely retained this *Bcl-2* deficiency
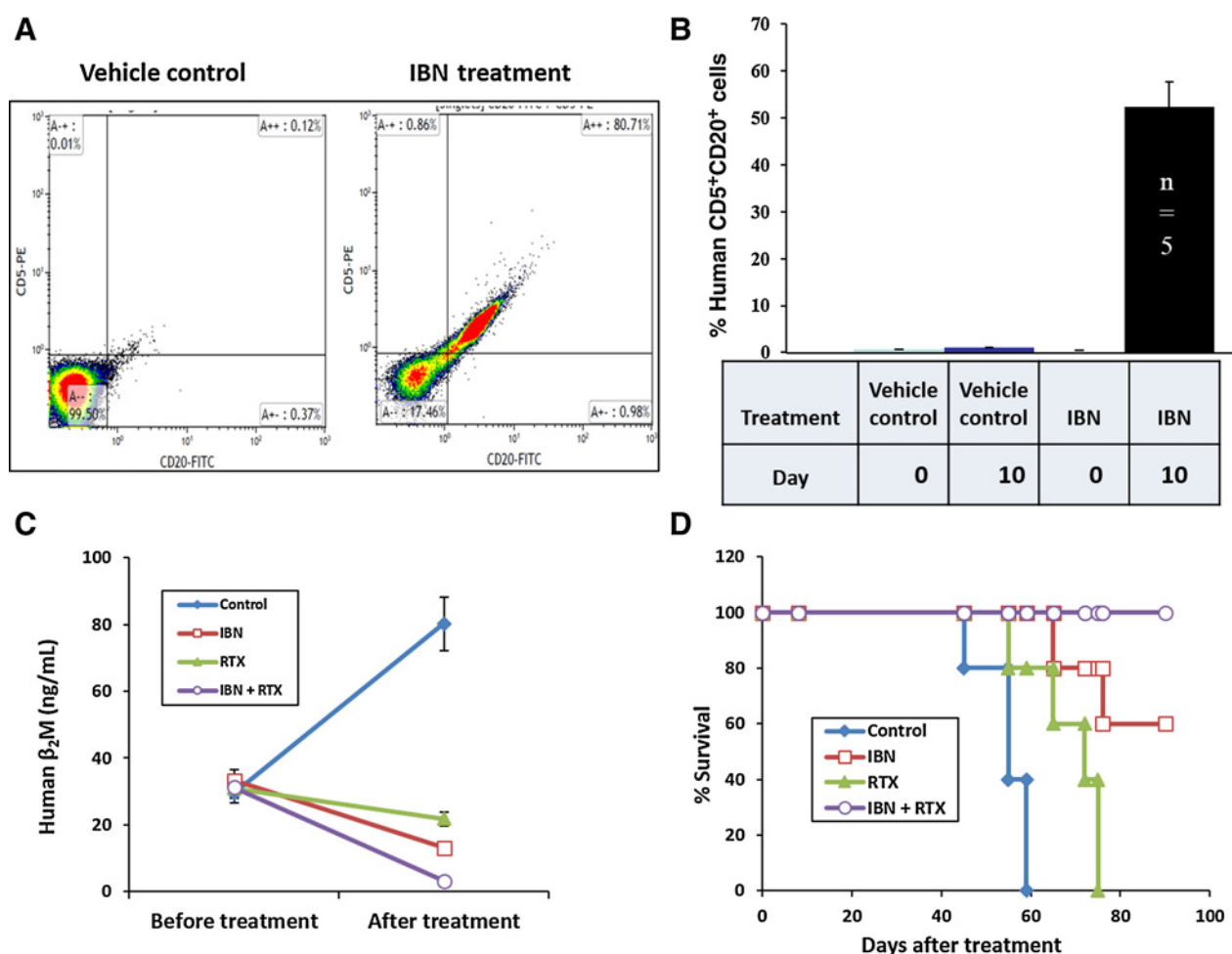
Figure 3.
Reproduction of the clinical compartmental shift phenomenon and the identification of novel combination therapy with PDX models. Freshly isolated MCL cells from the peripheral blood of PT5 were directly engrafted into the human fetal bone chips of SCID-hu G1 mice. The engrafted MCL cells produced measurable levels of human β_2M in mouse serum. Once human β_2M was detected in the mouse serum, PDX G1 mice were treated with 25 mg/kg IBN oral gavage daily. **A,** Representative flow cytometry data; **B,** pooled data showed that IBN induced a shift of human $CD5^+CD20^+$ cells from the area surrounding the implanted bone chip to the mouse peripheral blood on day 10 of treatment (vehicle control vs. IBN, $P < 0.01$). Once a transient increase of human $CD5^+CD20^+$ cells in mouse peripheral blood was detected, 10 mg/kg RTX was intravenously administered alone or combined with IBN every 3 days for total 7 doses. **C,** Tumor burden was monitored by human β_2M levels in mouse serum before treatment (day 0) and after treatment (day 30; $P < 0.01$, IBN plus RTX vs. vehicle control or RTX; $P < 0.05$, IBN plus RTX vs. IBN). **D,** Kaplan–Meier survival curves of primary MCL-bearing SCID-hu mice were analyzed ($P < 0.01$, IBN plus RTX vs. vehicle control, RTX, or IBN). RTX, rituximab; IBN, ibrutinib.

during multiple generations of tumor passage. These results demonstrated that the PDX model reliably displayed a drug resistance pattern that accurately reflected the disease biology of the patients.

PT8 was a patient with relapsed/refractory MCL who had clinical primary resistance to ibrutinib. We validated this resistance to ibrutinib by testing *in vitro* growth inhibition of the primary patient tumor cells (Fig. 4D) and PT8-MCL cells isolated from PDX tumors of G2 (Fig. 4E) and G3 (Fig. 4F). In addition, the *in vitro* growth inhibition data showed that these MCL cells from the PT8 primary patient sample and PDX tumors were sensitive to carfilzomib or ABT-199 (Fig. 4D–F). Furthermore, carfilzomib completely inhibited tumor growth in PT8-MCL-G3 PDX mice, indicating that carfilzomib inhibited the tumor growth of a primary ibrutinib-resistant tumor *in vivo* using a PDX mouse model (Supplementary Fig. S4).

PT12 was a patient with newly diagnosed ABC-type DLBCL. The tumor cells from the original patient, PDX-G2, and PDX-G3 of PT12 showed the same drug response pattern (Fig. 4G–I). Taken together, these results demonstrated that PDX models can be used to examine the effects of small-molecule–targeted agents *in vitro* with eventual validation *in vivo*.

Targeting PI3K or the proteasome against ibrutinib resistance

PT1-MCL was confirmed ibrutinib-sensitive by *in vitro* testing of the primary tumor cells, and the PDX was established and passaged to subsequent generations. Beginning in G3, the PT1-MCL PDX mice were exposed to ibrutinib by daily oral gavage to confer ibrutinib resistance as shown in Fig. 5A. This daily ibrutinib administration induced the development of an acquired ibrutinib-resistant tumor in PDX-G4. The cell viability of isolated PDX
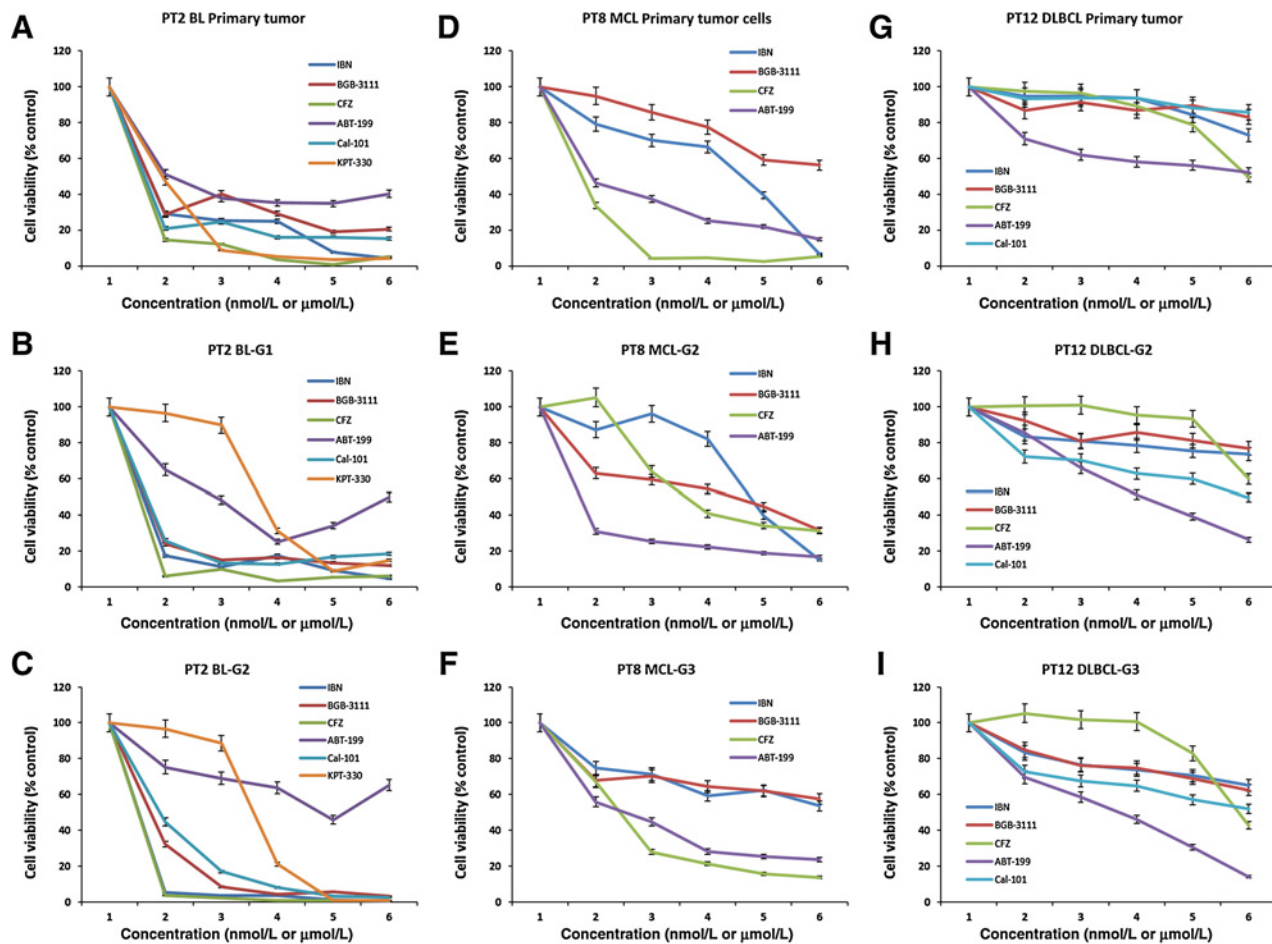
Figure 4.
Treatment profiling of freshly isolated tumor cells from patient samples and PDXs. **A–C,** Freshly isolated lymphoma cells from PT2-BL primary tumor, PDX-G1 tumor, and PDX-G2 tumor. **D–F,** Freshly isolated lymphoma cells from PT8-MCL primary tumor, PDX-G2 tumor, and PDX-G3 tumor. **G–I,** Freshly isolated lymphoma cells from PT12-DLBCL primary tumor, PDX-G2 tumor, and PDX-G3 tumor. Cell viability was tested by CellTiter-Glo luminescent cell viability assay after 48-hour incubation with indicated drug treatment. The dose ranges from 1 to 6 represent: IBN, BGB-3111, and Cal-101 at 0, 1.5, 3.1, 6.25, 12.5, 25 µmol/L; CFZ and ABT-199 at 0, 3.1, 6.25, 12.5, 25, 50 nmol/L; KPT-330 at 0, 0.07, 0.15, 0.3, 0.61, 1.25 µmol/L, respectively. Ibrutinib; CFZ, carfilzomib; PT, patient; BL, Burkitt's lymphoma; MCL, mantle cell lymphoma; DLBCL, diffuse large B-cell lymphoma. All the P-values were calculated using multiple linear regression models.

tumor cells treated with ibrutinib was not significantly different between G1 and G2 as well as between G5 and G6 (Fig. 5B, $P > 0.05$). However, the cell viability of the G5 and G6 tumor cells was significantly higher than of the G1 and G2 tumor cells after ibrutinib treatment ($P < 0.01$), indicating that the G5 and G6 tumor cells were resistant to ibrutinib. We also validated ibrutinib resistance *in vivo* by treating the PDX-G5 mice with vehicle control or ibrutinib (25 mg/kg, oral gavage daily). The tumor masses and PET-CT scans demonstrated no difference in tumor burden between the ibrutinib-treated mice and vehicle control mice (Fig. 5C, $P > 0.05$), indicating that acquired drug resistance was established in PDX-G5.

To identify the underlying mechanisms associated with acquired ibrutinib resistance, we first compared the protein expression profiles of the PDX samples before and after ibrutinib exposure by RPPA analysis. The RPPA data revealed that the downstream BTK signaling molecule PLC-γ2, the canonical NFκB protein p65, and Src (pY416) were downregulated in the ibruti-

nib-resistant PDX cells. Instead, a component of the PI3K catalytic subunit p110 (p110alpha) and members of the BCL-2 antiapoptotic family Bcl-xL and Mcl-1 were upregulated after consistent exposure to ibrutinib (Fig. 5D). These results suggest that alternative signaling pathways may underlie ibrutinib resistance. Next, we aimed to inhibit the PI3K pathway while continuing to inhibit BTK. To this end, we targeted the PI3K pathway with idelalisib (Cal-101), the FDA-approved agent for the treatment of CLL, SLL, and FL, which targets all PI3K p110 isoforms at varying IC_{50} values, in combination with ibrutinib. The *in vitro* data showed that the freshly isolated MCL cells from the G5 tumor mass of ibrutinib-exposed PDX mice were resistant to ibrutinib but the combination of ibrutinib with Cal-101 or carfilzomib overcame drug resistance after 48 hours of incubation with 10 µmol/L ibrutinib plus 10 µmol/L Cal-101 or 10 nmol/L carfilzomib (Fig. 5E; Control vs. IBN, carfilzomib, or Cal-101, $P > 0.05$; Control vs. IBN+Cal-101 or IBN+carfilzomib, $P < 0.01$). Next, the combination of ibrutinib with Cal-101 or carfilzomib effectively
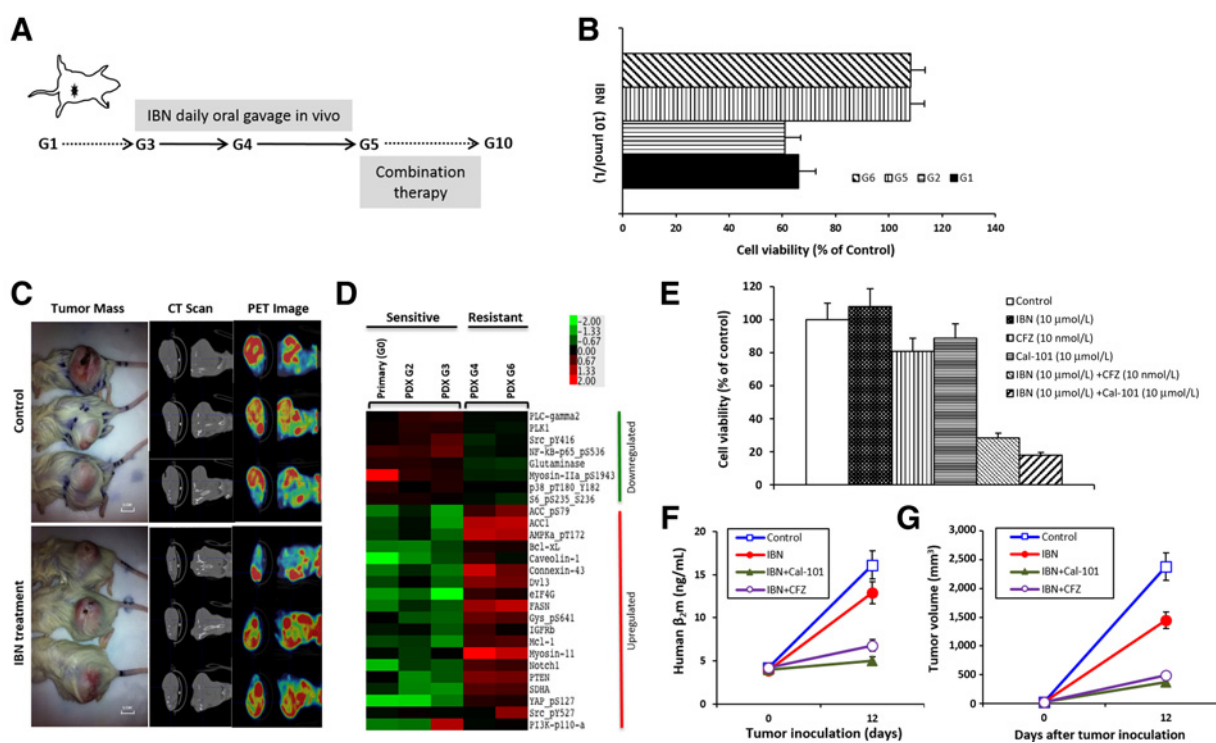
Figure 5.
The identification of treatment combinations to overcome ibrutinib resistance. **A,** Ibrutinib-naïve lymphoma cells were freshly isolated from apheresis of PT1-MCL. After PDX-G1 was established, the PDXs were passaged to next generations (G). Beginning in G3, the mice were treated with IBN (25 mg/kg, oral gavage daily). In G5, the mice were administered combination therapy to overcome drug resistance. **B,** Lymphoma cells were freshly isolated from G1, G2, G5, and G6 PDX tumors. Cell viability was tested by CellTiter-Glo luminescent cell viability assay after 48-hour incubation with 10 μmol/L IBN. Cell viability in G5 and G6 was much higher than in G1 and G2 ($P < 0.01$), indicating that the PDX acquired IBN resistance in G5. **C,** The gross tumor mass, CT scan, and PET image showed no difference of tumor burden between vehicle control and ibrutinib-treated mice ($P > 0.05$, $n = 3$), validating the acquired resistance to IBN in PDX-G5. **D,** RPPA data showed the upregulation and downregulation of lymphoma-associated signaling pathways in IBN-sensitive and IBN-resistant tumor samples. **E,** The freshly isolated MCL cells from the G5 tumor mass were incubated with 10 μmol/L IBN, 10 μmol/L Cal-101, 10 nmol/L CFZ, or 10 μmol/L IBN plus 10 μmol/L Cal-101 or 10 nmol/L CFZ for 48 hours. Cell viability was tested by CellTiter-Glo luminescent cell viability assay (Control vs. IBN, CFZ, or Cal-101, $P > 0.05$; Control vs. IBN+Cal-101 or IBN+CFZ, $P < 0.01$). **F,** Mice were administered with vehicle control, ibrutinib 25 mg/kg oral gavage daily, with/without Cal-101 25 mg/kg oral gavage daily, or CFZ 5 mg/kg i.v. on days 1 and 5. Mouse serum was collected from tail vein blood on days 1 and 12 of G5 tumor inoculation. Human β_2M was detected by ELISA for monitoring tumor burden (Control vs. IBN, $P = 0.25$; Control vs. IBN+Cal-101 or IBN+CFZ, $P < 0.01$). **G,** Tumor volumes were calculated for monitoring tumor burden (Control vs. IBN, $P = 0.25$; Control vs. IBN+Cal-101 or IBN+CFZ, $P < 0.01$). PT, patient; IBN, ibrutinib; CFZ, carfilzomib.

inhibited tumor growth of this ibrutinib-resistant tumor *in vivo* (Fig. 5F and G, ibrutinib vs. ibrutinib + Cal-101 or ibrutinib + carfilzomib, $P < 0.01$). These results indicated that even though the tumor was resistant to single-agent ibrutinib, targeting the PI3K pathway simultaneously with Cal-101 or targeting the proteasome downstream of PI3K signaling significantly inhibited tumor growth; therefore, simultaneous inhibition of the BCR signaling pathway and the PI3K signaling pathway or the proteasome may be an effective method to treat ibrutinib resistance.

Precision therapy guided by PDX models

We determined whether an established drug-resistant PDX model could precisely inform the therapeutic choices for an individual patient in the clinic. PT15 was an 88-year-old female with relapsed MCL (Table 1). Her treatment history included six cycles of R-CHOP, two cycles of rituximab plus bendamustine, rituximab, and bortezomib for 10 cycles, local radiation, resumption of rituximab and bendamustine for an additional six cycles,

and high-dose chemotherapy followed by autologous stem cell transplantation. The patient relapsed after short remissions from all of these therapies. However, the patient responded to ibrutinib single-agent treatment and was in complete remission for 3 years (green arrow in Fig. 6A). Once the patient relapsed from ibrutinib single-agent therapy (red arrow in Fig. 6A), the patient's PDX model was created using these now ibrutinib-resistant lymphoma cells.

After 79 days from the collection of PT15 MCL tumor cells, we isolated PT15-MCL-G2 cells and treated with a panel of drugs. We found that the G2 cells were most sensitive to bortezomib (BTZ, velcade) compared with other agents (Fig. 6B, $P \leq 0.002$). Bortezomib is FDA-approved for relapsed/refractory MCL; therefore, we were able to treat PT15 with a bortezomib-regimen guided by the PDX results (bortezomib, rituximab, and dexamethasone). The bortezomib-based regimen dramatically reduced the levels of tumor cells in the peripheral blood (lymphocytosis) of the patient (purple arrow in Fig. 6A). Taken
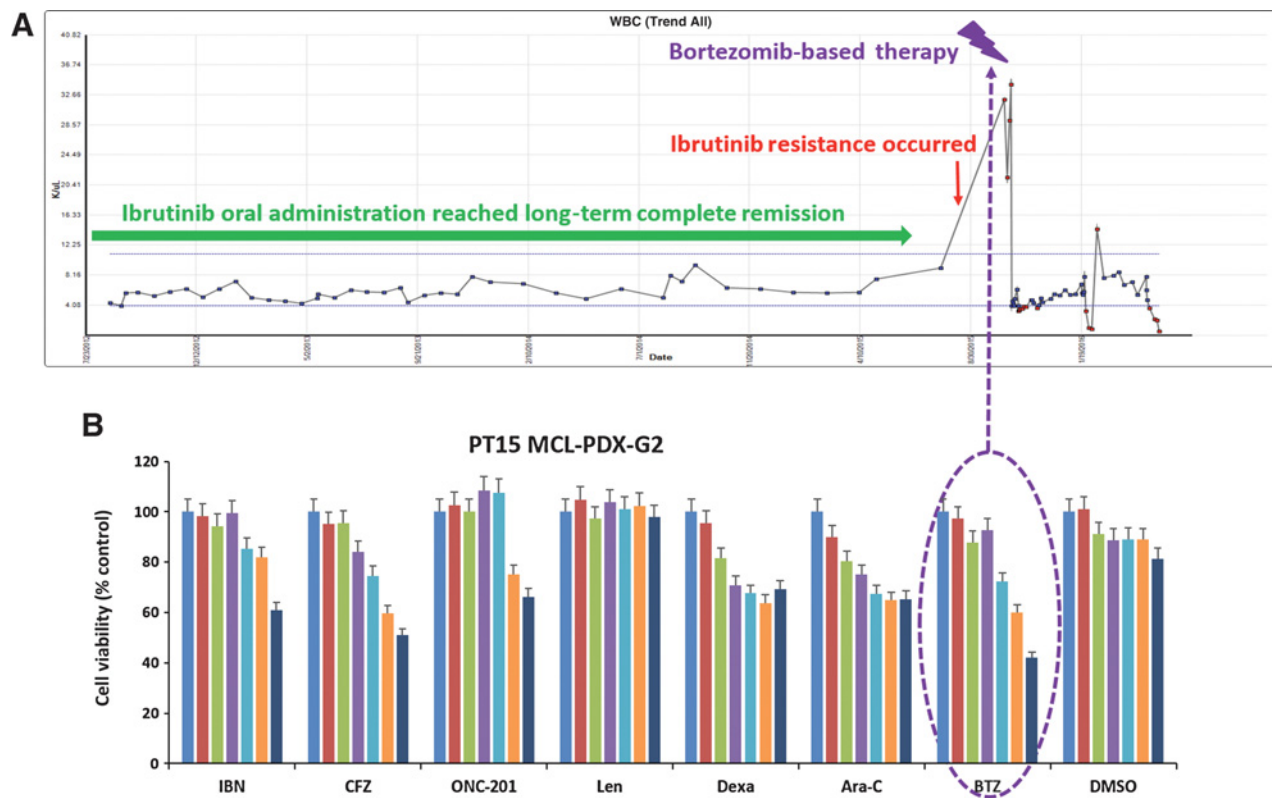
Figure 6.
PDX models precisely guide individual patient therapy in the clinic. **A,** Clinical responses of PT15. **B,** PT15-MCL-G2 tumor cells were freshly isolated and cell viability was tested using the CellTiter-Glo luminescent cell viability assay after 48-hour incubation with indicated drug treatments, with the G2 tumor cells showing sensitivity to BTZ. The *in vitro* drug and dosage information is listed in Supplementary Table S1. IBN, ibrutinib; BTZ, bortezomib; CFZ, carfilzomib; Len, lenalidomide; RTX, rituximab; Dexa, dexamethasone; PT, patient.

together, our data indicated that the PDX mouse model identified an efficacious therapy for a relapsed/refractory MCL patient, strongly suggesting that the PDX model is a valid experimental platform that can guide clinical decision-making with respect to therapeutic agents.

Discussion

Recent studies have shown a remarkable correlation between drug activity in PDXs and clinical outcomes when patients with advanced cancers were treated with selected regimens based on their PDX treatment responses (10, 24). These findings suggest that PDXs are a robust model to assess responses to novel drugs and can be used to predict clinical efficacies of treatment regimens. Furthermore, patient-derived primary cancer cell cultures (PDPC) from a biopsy sample were shown to retain tumor heterogeneity and were used to identify an effective therapy for a patient with respiratory papillomatosis (25). In addition, PDPCs have also been used to identify effective drug combinations to overcome resistance to targeted therapy in lung cancer (26). These studies provide the rationale that PDX-based adaptive therapy could be utilized to select a beneficial patient regimen.

In this study, we established 16 different B-cell lymphoma PDX models. The overall passage success rate was 67% in all of the PDX models. MCL-PDXs and DLBCL-PDXs had a 75% (6/8) and 67%

(2/3) success rate of passaging across multiple generations, respectively. These success rates are higher than other recently published B-cell lymphoma PDX models (8, 27). Specifically, Townsend and colleagues created a large, publicly available repository of leukemia and lymphoma patient-derived PDXs. The engraftment success rates by tail-vein injection were higher in acute lymphoblastic leukemias but lower in lymphomas. In addition, Townsend and colleagues implanted lymphoma tissue under the renal capsule with a 30.2% success rate and experienced difficulty in developing low-grade lymphoma models (27). Of note, we also successfully set up a PT2-BL-PDX model that was passaged across multiple generations, and the clinical pathology report showed a *Bcl-2* deficiency in the patient's original tumor. Correspondingly, PT2-BL tumor cells from the original patient sample displayed resistance to ABT-199. Furthermore, the PT2-BL PDX model reliably displayed resistance to ABT-199 even after 7 generations, suggesting that that the PDXs most likely maintained the *Bcl-2* deficiency across multiple generations.

To further elucidate the accurate reflection of genetic mutations in B-cell lymphoma PDXs compared with the original patient tumor, we investigated the genetic similarities of the PDX tumors by sequencing two sets of PDX models in comparison with the patient primary tumors. Only an additional Thr1627Met mutation in *DNAH5* was observed at 20% allele frequency in G3 of one PDX model compared with the patient tumor. This *DNAH5*

mutation has not been previously reported to be associated with B-cell lymphoma. These results suggest that these two PDXs maintained the original patient genetic profiles without the loss or accumulation of additional mutations.

Most B-cell lymphoma patients relapse after initial therapy, and secondary therapies are urgently needed to cause remission. Ibrutinib, a first-in-class, once-daily, oral BTK inhibitor, was approved by the FDA in 2013 to treat relapsed/refractory MCL. In our prior multiple-center phase II clinical trial, the overall response rate in relapsed/refractory MCL patients was 68%, with a median progression free survival (PFS) of 13.9 months, surpassing the effectiveness of other therapies (22). However, despite the dramatic responses to ibrutinib, resistance to ibrutinib inevitably develops. Moreover, the patients who initially show lengthy, durable responses to ibrutinib often acquire resistance and relapse at a median of 17 months. Once patients relapse after ibrutinib treatment, the 1-year survival rate is only 22% (28). Using the PDX model, we first established primary ibrutinib-resistant PDXs using tumor cells collected from PT8 and PT10, who were patients with relapsed/refractory MCL who had clinical primary resistance to ibrutinib. To identify regimens that can be potentially utilized to overcome primary ibrutinib resistance, we performed cell viability assays in vitro that showed that the tumor cells from PT8 PDX-G2 and PT8 PDX-G3, as well as the original primary tumor cells, were resistant to ibrutinib but sensitive to the proteasome inhibitor carfilzomib. Next, the in vivo data in PT8 PDX-G3 validated ibrutinib resistance and carfilzomib activity, demonstrating that the PDX model can be employed to identify regimens to treat therapeutic resistance.

We also established acquired ibrutinib-resistant PDXs by administering ibrutinib daily to G3 and G4 mice established using an ibrutinib-sensitive patient sample. In the acquired ibrutinib-resistant PDXs, PLC-γ2, p65, and Src were down-regulated; however, BCL-2 family members and a PI3K signaling component were up-regulated. Both BTK and PI3K are involved in proximal BCR signaling, and once the BTK-mediated effect became inactive due to desensitization to ibrutinib, the signals mediated by the PI3K pathway may possibly promote growth and survival (29). Finally, our in vivo data showed that the combination of ibrutinib with idelalisib, as well as with its combination with carfilzomib, resulted in halting tumor growth in vivo. The results suggest that PDXs can be used as a translational model to explore alternative therapies and drug combinations in the context of acquired drug resistance. These findings support the results observed in ibrutinib-resistant chronic lymphocytic leukemia (CLL; ref. 30).

We also created an ibrutinib-resistant PDX mouse model using the clinically acquired resistant PT15 tumor cells. The preclinical data obtained in this model guided the therapy of the patient, dramatically reducing the patient's lymphocytosis. Furthermore, we calculated the mean passage time per generation across five generations for 10 B-cell lymphoma PDX mouse models and found that the mean passage time of 3 of 10 models was less than 1 month and the mean time ranged from 30 to 40 days for 4 models (Supplementary Table S4). These data support the use of PDX mouse models to provide personalized therapy to individual patients as previously reported by Hidalgo and colleagues (24). Hidalgo and colleagues reported a pilot study in which treatments for patients with advanced solid tumors were selected based on

the activity of novel agents against the corresponding PDX model. They observed a response rate of 88% for treatment(s) deemed effective by the model that were subsequently chosen for the patients (24). In addition, Stebbing and colleagues demonstrated the effectiveness of developing personalized therapies for rare tumors such as sarcomas. A correlation between the PDX results and clinical outcome was observed in 13 of 16 (81%) sarcoma patients, with no patients progressing during the PDX-predicted therapy (31). The previous reports along with our results discussed here strongly indicate that B-cell lymphoma PDXs can be used as a personalized therapy platform.

In this study, PDXs identified novel treatment choices that overcame drug resistance. Furthermore, the correlations between drug resistance and effective treatment responses may ultimately help identify biomarkers that can potentially predict effective treatment outcomes, ultimately personalizing therapy for B-cell lymphoma patients.

Disclosure of Potential Conflicts of Interest

S. Kadri is a consultant/advisory board member for GLG consulting. No potential conflicts of interest were disclosed by the other authors.

Authors' Contributions

Conception and design: L. Zhang, K. Nomie, Jack Wang, Jacqueline Wang, L. Li, Q. Yi, M. Wang
Development of methodology: L. Zhang, K. Nomie, H. Zhang, W. Tao, Jacqueline Wang, M. Wang
Acquisition of data (provided animals, acquired and managed patients, provided facilities, etc.): L. Zhang, H. Zhang, L. Pham, S. Li, D. Santos, W. Chen, O. Oriabure, Y. Liu, H. Guo, C. Li, Jack, Jacqueline Wang, S. Thirumurthi, S.Y. Huang, Y. Shao, Y.L. Wang, M. Wang
Analysis and interpretation of data (e.g., statistical analysis, biostatistics, computational analysis): L. Zhang, K. Nomie, H. Zhang, L. Pham, S. Kadri, J. Segal, S. Zhou, S. Sharma, Jacqueline Wang, Y.L. Wang, M. Wang
Writing, review, and/or revision of the manuscript: L. Zhang, K. Nomie, T. Bell, S. Li, S. Zhou, S. Huang, B. Fang, Jacqueline Wang, M. Ahmed, S.Y. Huang, Y.L. Wang, M. Wang
Administrative, technical, or material support (i.e., reporting or organizing data, constructing databases): L. Zhang, T. Bell, O. Oriabure, S. Huang, Z. Chen, M. Badillo, L. Lam, Y.L. Wang, M. Wang
Study supervision: L. Zhang, K. Nomie, B. Fang, M. Wang
Other (pathology review and picture taken): S. Li
Other (collection of tissue specimens): D. Santos
Other (ran all the next-generation sequencing (NGS) experiments for the samples using the hybrid capture panel and also helped in the NGS data interpretation): S. Sharma

References

1. Armitage JO, Weisenburger DD. New approach to classifying non-Hodgkin's lymphomas: clinical features of the major histologic subtypes. Non-Hodgkin's Lymphoma Classification Project. J Clin Oncol 1998;16: 2780–95.
2. Rovira J, Valera A, Colomo L, Setoain X, Rodríguez S, Martínez-Trillos A, et al. Prognosis of patients with diffuse large B cell lymphoma not reaching complete response or relapsing after frontline chemotherapy or immunochemotherapy. Ann Hematol 2015;94:803–12.
3. Shankland KR, Armitage JO, Hancock BW. Non-Hodgkin lymphoma. Lancet 2012;380:848–57.
4. Romaguera JE, Fayad LE, Feng L, Hartig K, Weaver P, Rodriguez MA, et al. Ten-year follow-up after intense chemoimmunotherapy with Rituximab-HyperCVAD alternating with Rituximab-high dose methotrexate/cytarabine (R-MA) and without stem cell transplantation in patients with untreated aggressive mantle cell lymphoma. Br J Haematol 2010;150: 200–8.
5. Cai Q, Chen Y, Zou D, Zhang L, Badillo M, Zhou S, et al. Clinical outcomes of a novel combination of lenalidomide and rituximab followed by stem cell transplantation for relapsed/refractory aggressive B-cell non-hodgkin lymphoma. Oncotarget 2014;5:7368–80.
6. Maddocks K, Christian B, Jaglowski S, Flynn J, Jones JA, Porcu P, et al. A phase 1/1b study of rituximab, bendamustine, and ibrutinib in patients with untreated and relapsed/refractory non-Hodgkin lymphoma. Blood 2015;125:242–8.
7. Williams SA, Anderson WC, Santaguida MT, Dylla SJ. Patient-derived xenografts, the cancer stem cell paradigm, and cancer pathobiology in the 21st century. Lab Invest 2013;93:970–82.
8. Chapuy B, Cheng H, Watahiki A, Ducar MD, Tan Y, Chen L, et al. Diffuse large B-cell lymphoma patient-derived xenograft models capture the molecular and biological heterogeneity of the disease. Blood 2016;127: 2203–13.
9. Tentler JJ, Tan AC, Weekes CD, Jimeno A, Leong S, Pitts TM, et al. Patient-derived tumour xenografts as models for oncology drug development. Nat Rev Clin Oncol 2012;9:338–50.
10. Morelli MP, Calvo E, Ordonez E, Wick MJ, Viqueira BR, Lopez-Casas PP, et al. Prioritizing phase I treatment options through preclinical testing on personalized tumorgraft. J Clin Oncol 2012;30:e45–8.
11. Zhang X, Claerhout S, Prat A, Dobrolecki LE, Petrovic I, Lai Q, et al. A renewable tissue resource of phenotypically stable, biologically and ethnically diverse, patient-derived human breast cancer xenograft models. Cancer Res 2013;73:4885–97.
12. Marangoni E, Vincent-Salomon A, Auger N, Degeorges A, Assayag F, de Cremoux P, et al. A new model of patient tumor-derived breast cancer xenografts for preclinical assays. Clin Cancer Res 2007;13:3989–98.
13. Topp MD, Hartley L, Cook M, Heong V, Boehm E, McShane L, et al. Molecular correlates of platinum response in human high-grade serous ovarian cancer patient-derived xenografts. Mol Oncol 2014;8:656–68.
14. Wang M, Zhang L, Han X, Yang J, Qian J, Hong S, et al. A severe combined immunodeficient-hu in vivo mouse model of human primary mantle cell lymphoma. Clin Cancer Res 2008;14:2154–60.
15. Tarella C, Gueli A, Delaini F, Rossi A, Barbui AM, Gritti G, et al. Rate of primary refractory disease in B and T-cell non-Hodgkin's lymphoma: correlation with long-term survival. PLoS One 2014;9:e106745.
16. Conlan MG, Bast M, Armitage JO, Weisenburger DD. Bone marrow involvement by non-Hodgkin's lymphoma: the clinical significance of morphologic discordance between the lymph node and bone marrow. Nebraska Lymphoma Study Group. J Clin Oncol 1990;8:1163–72.
17. Bassarova A, Troen G, Spetalen S, Micci F, Tierens A, Delabie J. Lympho-plasmacytic lymphoma and marginal zone lymphoma in the bone marrow paratrabecular involvement as an important distinguishing feature. Am J Clin Pathol 2015;143:797–806.
18. Goldman S, Smith L, Galardy P, Perkins SL, Frazer JK, Sanger W, et al. Rituximab with chemotherapy in children and adolescents with central nervous system and/or bone marrow-positive Burkitt lymphoma/leukaemia: a Children's Oncology Group Report. Br J Haematol 2014;167: 394–401.
19. Yan Y, Chan WC, Weisenburger DD, Anderson JR, Bast MA, Vose JM, et al. Clinical and prognostic significance of bone marrow involvement in patients with diffuse aggressive B-cell lymphoma. J Clin Oncol 1995;13: 1336–42.
20. Sovani V, Harvey C, Haynes AP, McMillan AK, Clark DM, O'Connor SR. Bone marrow trephine biopsy involvement by lymphoma: review of histopathological features in 511 specimens and correlation with diagnostic biopsy, aspirate and peripheral blood findings. J Clin Pathol 2014;67:389–95.
21. The 1000 Genomes Project Consortium. An integrated map of genetic variation from 1,092 human genomes. Nature 2012;491:56–65.
22. Wang ML, Rule S, Martin P, Goy A, Auer R, Kahl BS, et al. Targeting BTK with ibrutinib in relapsed or refractory mantle-cell lymphoma. N Engl J Med 2013;369:507–16.
23. Wang ML, Lee H, Chuang H, Wagner-Bartak N, Hagemeister F, Westin J, et al. Ibrutinib in combination with rituximab in relapsed or refractory mantle cell lymphoma: a single-centre, open-label, phase 2 trial. Lancet Oncol 2016;17:48–56.
24. Hidalgo M, Bruckheimer E, Rajeshkumar NV, Garrido-Laguna I, De Oliveira E, Rubio-Viqueira B, et al. A pilot clinical study of treatment guided by personalized tumorgrafts in patients with advanced cancer. Mol Cancer Ther 2011;10:1311–6.
25. Yuan H, Myers S, Wang J, Zhou D, Woo JA, Kallakury B, et al. Use of reprogrammed cells to identify therapy for respiratory papillomatosis. N Engl J Med 2012;367:1220–7.
26. Crystal AS, Shaw AT, Sequist LV, Friboulet L, Niederst MJ, Lockerman EL, et al. Patient-derived models of acquired resistance can identify effective drug combinations for cancer. Science 2014;346:1480–6.
27. Townsend EC, Murakami MA, Christodoulou A, Christie AL, Koster J, DeSouza TA, et al. The public repository of xenografts enables discovery and randomized phase II-like trials in mice. Cancer Cell 2016;30:183.
28. Cheah CY, Chihara D, Romaguera JE, Fowler NH, Seymour JF, Hagemeister FB, et al. Patients with mantle cell lymphoma failing ibrutinib are unlikely to respond to salvage chemotherapy and have poor outcomes. Ann Oncol 2015;26:1175–9.
29. Suzuki H, Matsuda S, Terauchi Y, Fujiwara M, Ohteki T, Asano T, et al. PI3K and Btk differentially regulate B cell antigen receptor-mediated signal transduction. Nat Immunol 2003;4:280–6.
30. Cheng S, Guo A, Lu P, Ma J, Coleman M, Wang YL. Functional characterization of BTKC481S mutation that confers ibrutinib resistance: exploration of alternative kinase inhibitors. Leukemia 2015;29:895–900.
31. Stebbing J, Paz K, Schwartz GK, Wexler LH, Maki R, Pollock RE, et al. Patient-derived xenografts for individualized care in advanced sarcoma. Cancer 2014;120:2006–15.